Functional ultrasound imaging of the brain

Emilie Macé[1], Gabriel Montaldo[1], Ivan Cohen[2], Michel Baulac[2], Mathias Fink[1] & Mickael Tanter[1]

We present functional ultrasound (fUS), a method for imaging transient changes in blood volume in the whole brain at better spatiotemporal resolution than with other functional brain imaging modalities. fUS uses plane-wave illumination at high frame rate and can measure blood volumes in smaller vessels than previous ultrasound methods. fUS identifies regions of brain activation and was used to image whisker-evoked cortical and thalamic responses and the propagation of epileptiform seizures in the rat brain.

The common functional brain imaging modalities, including functional magnetic resonance imaging (fMRI) and positron emission tomography, have excellent depth penetration but do not provide good spatial and temporal resolution, which are critical when imaging complex transient events such as epileptic seizures. By contrast, ultrasound imaging achieves good spatiotemporal resolution in depth, but its poor sensitivity has until now limited its use to the imaging of major vessels. To overcome this limitation, we have developed functional ultrasound (fUS), a technique that is capable of imaging whole-brain microvasculature dynamics in response to brain activation with high spatiotemporal resolution.

Ultrasound imaging exposes a part of the body to pulsed ultrasonic waves and displays the amplitude of the ultrasonic echoes backscattered by tissues or fluids (**Fig. 1a**). Conventional ultrasound techniques scan the tissue line by line with a focused beam (**Supplementary Fig. 1**). This process is too slow to acquire large-field images (on the order of centimeters) at a kilohertz frame rate. However, a frame rate of that magnitude is critical for imaging blood dynamics by ultrasound. As a consequence, imaging blood dynamics by conventional ultrasound requires dividing the imaging field into smaller parts that are scanned successively, a process that permits the acquisition of only a limited number of samples (typically 8–15) per pixel[1] and therefore limits the sensitivity. Until now, this has restricted the application of conventional ultrasound to imaging of the main arteries.

In fUS, we use plane-wave illumination as opposed to focused beam scanning. We obtained a large-field image (2 cm × 2 cm) from a single plane-wave emission in the same acquisition time as one focused beam, allowing us to increase the number of samples acquired per pixel (**Fig. 1a** and **Supplementary Fig. 1**). Moreover, by using a set of tilted planar illuminations and coherently summing the resulting set of images (**Fig. 1b**), we produced a 'compound' ultrasonic image that had better resolution and lower noise than a conventional image, preserving a kilohertz frame rate[2,3].We performed fUS by acquiring 200 compound images at 1 kHz, each one from 17 planar illuminations tilted from −8° to 8°. The recent development of ultrafast ultrasound scanners made this technologically possible[4]. Using a 15-MHz ultrasound probe, we achieved a spatial resolution of 100 µm × 100 µm in the imaging plane, a slice thickness of 200 µm and a penetration depth (>2 cm) sufficient to image the whole rat brain in a very short acquisition time (200 ms).

The ultrasound scanner outputs the temporal course of the ultrasonic echoes' amplitude for each pixel $s(x,z,t)$ (**Fig. 1c**). During imaging of the blood, the pixel amplitude $s(t)$ fluctuates over time as a result of the movement of red blood cells with a characteristic frequency known as the Doppler frequency f_D[1] (Online Methods). Because of cardiac pulsatility and respiration, tissue motion is never zero, which also causes pixel amplitude fluctuations but of lower frequency than those due to blood motion. The blood signal $s_B(t)$ from $s(t)$ can therefore be extracted by applying a high-pass filter (**Fig. 1c**). From $s_B(t)$, two different hemodynamic parameters are usually estimated (**Fig. 1d**). Here we chose to measure the 'power Doppler'—defined as the mean intensity I of $s_B(t)$—which is proportional to the blood volume[5] (**Fig. 1d** and **Supplementary Note 1**). We can also calculate the axial blood velocity[1,6] from f_D, but because the mean frequency estimators are unstable in the presence of noise[1,5], the power Doppler is more suitable for imaging microvascular hemodynamics.

In the rat brain, blood velocities range from <1 mm s^{-1} in the capillaries to several centimeters per second in the arteries[7,8]. Consequently, when ultrasound is emitted at 15 MHz, Doppler frequencies lie between 20 and 400 Hz, which means that one needs to acquire ultrasonic images at a high rate (>800 Hz) to sample $s(t)$ correctly. To exclude signals due to tissue motion, we set the cutoff frequency of the filter at 70 Hz. This necessary filtering step imposes a low limit: we can detect only red blood cells with an axial velocity >4 mm s^{-1}. Therefore, using fUS we can measure changes in blood volume in vessels that are flowing with speeds higher than this limit.

We performed an experimental comparison between power Doppler images obtained using conventional focused beam scanning ultrasound and fUS on the rat brain (**Supplementary Fig. 1**). We calculated the sensitivity of power Doppler imaging as being proportional to the noise I_η on each sample and inversely

[1]Institut Langevin, Ecole Supérieure de Physique et de Chimie Industrielles Paris Tech, Centre National de la Recherche Scientifique (CNRS) UMR7587, Institut National de la Santé et de la Recherche Médicale (INSERM) U979, Université Paris VII, Paris, France. [2]Centre de Recherche Institut du Cerveau et de la Moelle Epinière, INSERM UMRS 975, CNRS UMR7225, Centre Hospitalier Universitaire Pitié Salpêtrière, Paris, France. Correspondence should be addressed to M.T. (mickael.tanter@espci.fr).

RECEIVED 3 DECEMBER 2010; ACCEPTED 27 MAY 2011; PUBLISHED ONLINE 3 JULY 2011; DOI:10.1038/NMETH.1641

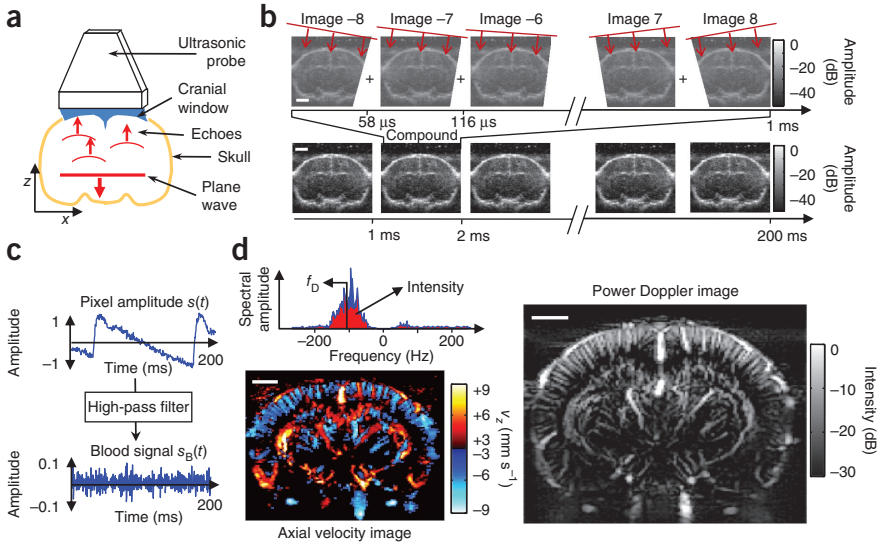

Figure 1 | Principles for performing fUS in the rat brain. (**a**) Schematic setup depicting the ultrasonic probe, cranial window and a schema of a coronal slice from the rat brain. The principles of ultrasound imaging are schematized. (**b**) fUS is performed by emitting 17 planar ultrasonic waves tilted with different angles into the rat brain. The ultrasonic echoes produce 17 images of 2 cm × 2 cm (amplitudes are in decibels, dB). Summing up these images results in a compound image acquired in 1 ms. The entire fUS sequence consists of acquiring 200 compound images in 200 ms. (**c**) Temporal variation $s(t)$ of the backscattered ultrasonic amplitude in one pixel (normalized by the maximum amplitude). The blood signal s_B is extracted by applying a high-pass filter (same scale in the two graphs). (**d**) Frequency spectrum of s_B (top left). Two parameters are extracted from this spectrum: the central frequency f_D, which is proportional to the axial blood velocity with respect to the z axis and gives rise to the axial velocity image (below left); and the intensity (power Doppler), which is proportional to the cerebral blood volume and gives rise to the power Doppler image (right). fUS is based on power Doppler images. Scale bars, 2 mm.

proportional to the square root of N, the number of samples acquired in $s_B(t)$ (**Supplementary Note 2**). I_η was measured to be 9 times lower and N to be 13 times higher in fUS compared to conventional US. Therefore, fUS increased the sensitivity of the power Doppler by a factor of 47 (**Supplementary Note 2**). This increased sensitivity makes it possible to measure blood volumes in smaller vessels. The high temporal and spatial resolution coupled with high depth penetration of fUS make it an ideal method for performing functional brain imaging.

We therefore used fUS to image task-evoked brain activation. fUS determines regions of brain activity based on increased blood volume due to neurovascular coupling. We performed fUS acquisitions every 3 s on trepanned rats (n = 6) during whisker stimulation (**Fig. 2a**). (It would be possible to reduce the time between acquisitions to 200 ms with a scanner of higher computing power.) Stimulation of groups of vibrissae resulted in a steady increase in blood volume in the primary somatosensory barrel cortex (S1), with increases in the power Doppler signal ranging from 10% to 20% during the stimuli (**Fig. 2a**). Maps of activated pixels were built showing the correlation coefficient r between the power Doppler signal and the temporal pattern of the stimulus (Online Methods and **Supplementary Fig. 2**). Activation maps

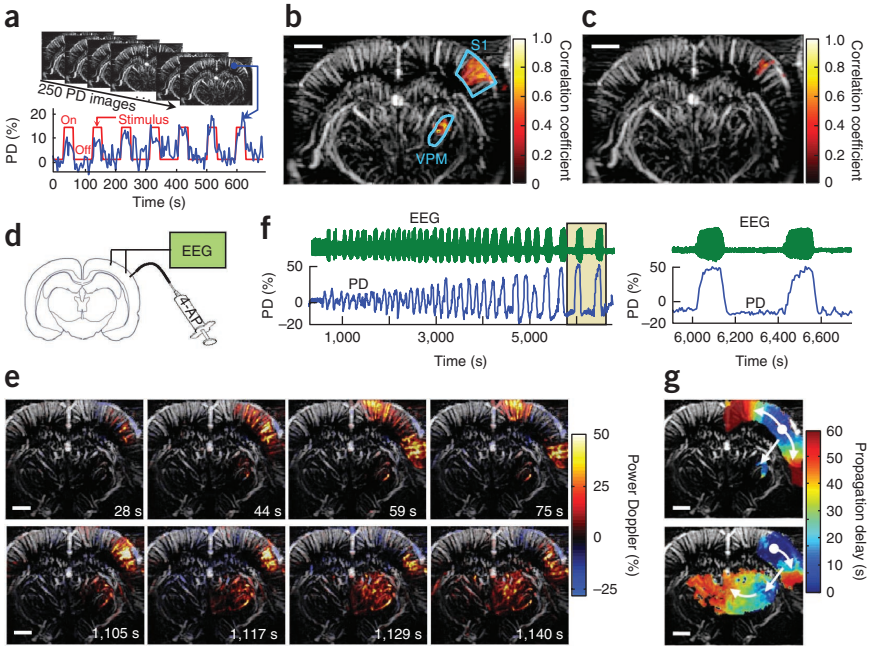

Figure 2 | Applications of fUS imaging. (**a**–**c**) fUS imaging of task-evoked brain activation in the rat brain. (**a**) Power Doppler (PD) fUS images are acquired every 3 s during whisker stimulation (probe in the coronal plane, stereotaxic coordinates β –2.5 mm). The whisker stimulation pattern (red line) consisted of 32 s on and 64 s off repeated 10 times (7 cycles shown). The PD is plotted in percentage relative to the baseline (n = 6). (**b**) Representative example of an activation map obtained when stimulating the left whiskers. We calculated maps as the correlation coefficient between the power Doppler signal and the stimulus pattern. S1, primary somatosensory barrel cortex; VPM, ventral posterior medial nucleus. S1 and VPM regions were delineated from a rat brain atlas. (**c**) Representative example of an activation map obtained when stimulating a single whisker. (**d**–**g**) fUS imaging of transient brain activity in a rat model of epilepsy. (**d**) Schematic setup for the imaging of epileptiform seizures. We injected 4-AP focally in the cortex and implanted cortical electrodes for EEG recordings (n = 4). (**e**) Spatiotemporal spreading of epileptiform activity for two selected ictal events. The power Doppler signal (in percentage relative to baseline) is superimposed on a control power Doppler image. (**f**) Comparison between electrical recordings (EEG; green line) and the power Doppler signal (PD, blue line) at the site of 4-AP injection. The two events in the shaded region are zoomed in on the graph at right. (**g**) Maps of the propagation delay of blood volume changes from the focus to other regions (propagation delay in seconds is color coded following the legend on the right: onset is indicated in blue; and blue to red indicates delay increases). Arrows represent the direction of propagation. Scale bars, 2 mm.

(**Fig. 2b**) show a significant activation of S1 ($r > 0.2$, Online Methods) during whisker stimuli. We also detected a significant activation ($r > 0.2$) in the ventral posterior medial nucleus (VPM) of the thalamus, a region that makes thalamocortical connections with S1 (ref. 9) and that becomes activated during whisker stimulation[10]. To further test the sensitivity of fUS, we repeated these experiments by deflecting a single whisker to activate an individual cortical column in S1. Activation maps obtained from ten trials (**Fig. 2c**) show significant activation ($r > 0.2$) of a small S1 region.

The high spatiotemporal resolution of fUS for imaging task-evoked activation is notable compared to those of other functional imaging modalities. By contrast, fMRI can reach similar spatial resolution, but its temporal resolution is slower (on the order of seconds) and is intrinsically linked to the size of the voxel[11]. Greater speed is not, in theory, critical for functional imaging because neurovascular coupling is slow, but it does provide extra time to acquire more slices or to increase averaging. Beyond the gain in resolution, an important benefit of fUS over fMRI lies in its high sensitivity for detecting hemodynamic responses, as demonstrated by the low noise observed in the activation maps (**Supplementary Fig. 2**). Because of the low signal-to-noise ratio of fMRI, averaging across multiple trials becomes necessary, and therefore imaging transient events remains a challenge[12].

To evaluate the potential of fUS for imaging transient brain activity, we performed fUS in a rat model of epilepsy ($n = 4$). We induced acute ictogenesis by the focal injection of a potassium channel blocker (4-aminopyridine, 4-AP) in the cortex of a trepanned rat while performing fUS acquisitions every 3 s (**Fig. 2d**). We were thereby able to image the dynamics of blood volume in response to epileptiform activity (**Supplementary Video 1**), representing—to our knowledge—the first time that an epileptic seizure has been imaged in the whole brain at such spatiotemporal resolution[13]. The video shows the onset of blood volume increases at the injection site followed by diffuse and bilateral spreading, such as occurred in the four experiments. In this representative example, we observed different spreading patterns of blood volume changes such as cortical waves crossing in both hemispheres, localized ipsilateral corticothalamic activations or a wave traveling through the whole thalamus (two examples from this video are shown in **Fig. 2e**).

To verify that epileptic neuronal activity underlies the changes in blood volume observed, we performed extracellular cortical recordings simultaneously with fUS imaging. In all four animals, we implanted eight electrodes at different positions in the cortex and measured localized increases in blood volume during ictal periods. In a representative example of the power Doppler and electric signals recorded at the injection site during a seizure (**Fig. 2f**), the power Doppler value increased between 15% and 50% during ictal activity compared to the baseline. Moreover, the power Doppler signal was highly correlated with the envelope of the electroencephalogram (EEG) signal ($r = 0.87$).

We then investigated the spreading velocity of ictal activity, by measuring the propagation time of surrogate blood volume responses from a reference point to other pixels (Online Methods and **Supplementary Fig. 3**). **Figure 2g** shows delay maps of the two examples previously shown in **Figure 2e**. We measured the wave traveling speed for one ictal event and found that the cortical waves travel at a speed of 3.2 ± 0.3 mm min^{-1} and the thalamic wave at a higher speed of 6.8 ± 0.3 mm min^{-1} (Online Methods). The speed range of cortical waves was similar to previous findings from studies of cortical spreading depression[14]. These results demonstrate the potential of fUS for identifying epileptic foci and for studying the mechanisms of seizure spreading *in vivo*.

The ability to image cerebral blood volume at high spatiotemporal resolution and with high sensitivity using fUS could be of great interest for applications in which fMRI reaches its limits, such as imaging of epileptic-induced changes in blood volume. fUS could potentially be applied for chronic studies in animal models through a thinned-skull[15] or smaller cranial window. In the future, fUS could be implemented on a portable ultrasound scanner, opening a wide range of possibilities for functional imaging. Miniaturization of the probe could enable its implantation in the brain of awake, behaving animals. Finally, in the clinic, fUS could be readily applied to babies in a noninvasive approach through the fontanel window or to adults during open-skull neurosurgery.

METHODS

Methods and any associated references are available in the online version of the paper at http://www.nature.com/naturemethods/.

Note: Supplementary information is available on the Nature Methods website.

ACKNOWLEDGMENTS

We thank A. Urban for helpful comments on the manuscript and for technical advice on surgery and T. Montaldo for critical editorial comments on the manuscript.

AUTHOR CONTRIBUTIONS

M.B., M.F. and M.T. conceived and initiated the project; M.T. supervised the project. E.M., G.M. and I.C. designed and performed experiments; E.M., G.M. and M.T. wrote the manuscript.

COMPETING FINANCIAL INTERESTS

The authors declare no competing financial interests.

Published online at http://www.nature.com/naturemethods/.
Reprints and permissions information is available online at http://www.nature.com/reprints/index.html.

1. Szabo, T.L. in *Diagnostic Ultrasound Imaging: Inside Out* 366–376 (Elsevier Academic Press, 2004).
2. Montaldo, G., Tanter, M., Bercoff, J., Benech, N. & Fink, M. *IEEE Trans. Ultrason. Ferroelectr. Freq. Control* **56**, 489–506 (2009).
3. Bercoff, J. *et al. IEEE Trans. Ultrason. Ferroelectr. Freq. Control* **58**, 134–147 (2011).
4. Fink, M. & Tanter, M. *Phys. Today* **63**, 28–33 (2010).
5. Rubin, J.M., Bude, R.O., Carson, P.L., Bree, R.L. & Adler, R.S. *Radiology* **190**, 853–856 (1994).
6. Bonnefous, O. & Pesqué, P. *Ultrason. Imaging* **8**, 73–85 (1986).
7. Fung, Y.C. in *Biomechanics: Circulation* 2nd edn., 275–283 (Springer, 1997).
8. Kleinfeld, D., Mitra, P.P., Helmchen, F. & Denk, W. *Proc. Natl. Acad. Sci. USA* **95**, 15741–15746 (1998).
9. Jensen, K.F. & Killackey, H.P. *J. Neurosci.* **7**, 3544–3553 (1987).
10. Nicolelis, M.A. & Chapin, J.K. *J. Neurosci.* **14**, 3511–3532 (1994).
11. Yang, X., Hyder, F. & Shulman, R.G. *Proc. Natl. Acad. Sci. USA* **93**, 475–478 (1996).
12. Logothetis, N.K. *Nature* **453**, 869–878 (2008).
13. DeSalvo, M.N. *et al. Neuroimage* **50**, 902–909 (2010).
14. Busija, D.W., Bari, F., Domoki, F., Horiguchi, T. & Shimizu, K. *Prog. Neurobiol.* **86**, 379–395 (2008).
15. Drew, P.J. *et al. Nat. Methods* **7**, 981–984 (2010).

ONLINE METHODS

Ultrasonic imaging. We used an Aixplorer ultrafast ultrasound scanner (Supersonic Imagine). This scanner acquires ultrasonic images from planar illuminations at a frame rate of up to 20 kHz for a 2-cm-deep image. It has 128 emission channels and 128 parallel reception channels. The reception sampling rate is 60 MHz, and the reception hardware filters range between 2 MHz and 30 MHz. The scanner provides a trigger signal for each ultrasonic event used for synchronization with whisker stimulation and with electroencephalography (EEG) recordings. We used a linear ultrasonic probe (Vermon) composed of 128 piezoelectric transducers spaced at a pitch of 100 µm. The probe is characterized by a central frequency of 14.4 MHz and a bandwidth of 6.8 MHz (47%). The surface of emission measures 12.8 mm × 3.5 mm, and the focal depth is 8.2 mm. The excitation voltage is 25 V. In some experiments we used a second probe with identical characteristics except for a pitch of 125 µm (wider field of view).

For the comparison between conventional Doppler US and fUS (**Supplementary Fig. 1**), we performed the two acquisition sequences successively using the same scanner and the same probe (pitch 125 µm). For the conventional US sequence, the scanner emitted 15 focused beams per line of the image (made of 128 lines) at a repetition rate of 1 kHz. The image was divided in 8 blocks of 16 lines to reach this frame rate. We set the focal depth of focused beams to 10 mm and the emission and reception apertures to 4 mm.

Processing of ultrasonic signals. After reception and beamforming of ultrasonic echoes by the scanner, we obtain complex ultrasonic images $s(x,z,t)$. If a scatterer in (x_0,z_0) moves toward the probe with an axial velocity v_z, the central frequency of the signal $s(x_0,z_0,t)$ is the Doppler frequency f_D defined as[16]

$$f_D = -\frac{2 f_0 v_z}{c}$$

where f_0 is the central frequency of the pulsed ultrasonic wave, v_z is the axial velocity (with the axis convention defined in **Fig. 1a**) and c is the speed of sound in the medium (1,540 m s^{-1} in tissue). We used Matlab software (MathWorks) to process the signals. To remove tissue signal, we used a numerical Butterworth high-pass filter of the fourth order with a cutoff frequency of 70 Hz. We calculated the power Doppler value I for each pixel as

$$I = \frac{1}{N}\sum_{i=1}^{N} s_B^2(t_i)$$

where N is the number of samples acquired and s_B the filtered signal.

For the axial velocity image presented in **Figure 1**, we estimated f_D as the first momentum of the power spectrum of the Doppler signal:

$$f_D = \frac{\int_{-f_S/2}^{f_S/2} f\left|S_B^2(f)\right| df}{\int_{-f_S/2}^{f_S/2}\left|S_B^2(f)\right| df}$$

where S_B is the Fourier transform of s_B and f_S is the frame rate (1 kHz)—that is, the sampling frequency of s_B. This estimator is unstable in regard to noise. In consequence, we masked the axial velocity image using power Doppler data to keep only the pixels with a sufficient intensity of blood signal (threshold applied: >−25 dB). A guide for implementation, codes and data examples on this software is provided as **Supplementary Software**.

Activation maps. Activation maps are given as maps of the Pearson's product-moment correlation coefficient r between the task pattern $A(t)$ and the power Doppler signal $s_B(t)$ for each pixel, defined as

$$r = \frac{\sum_{i=1}^{N_t}\left(s_B(t_i) - \hat{s}_B\right)\left(A(t_i) - \hat{A}\right)}{\sqrt{\sum_{i=1}^{N_t}\left(s_B(t_i) - \hat{s}_B\right)^2}\sqrt{\sum_{i=1}^{N_t}\left(A(t_i) - \hat{A}\right)^2}}$$

where ^ designates the mean value of the variable.

An example of a raw activation map (same data as **Fig. 2b**) is shown in **Supplementary Figure 2a**. For 10 cycles, the time course is composed of $N_t = 256$ independent time points.

We calculated z scores by applying a Fisher's transform, defined as

$$z = \frac{\sqrt{N_t - 3}}{2} \cdot \ln\frac{1+r}{1-r}$$

We chose a level of significance of $z > 3.1$ ($P < 0.001$, one-tailed test), which corresponds to $r > 0.193$. The map after threshold for the same example is shown in **Supplementary Figure 2c**. We identified brain structures (S1, VPM) using a rat brain atlas by performing a rigid registration of the corresponding coronal slice[17].

Delay maps. For each pixel, we estimated the propagation time of the blood volume response to epileptic activity between this pixel and a reference point. This propagation time is given by the position of the maximum of the correlation function between the two power Doppler signals (**Supplementary Fig. 3**).

Measurement of the spreading velocity. We aimed at measuring the velocity of a spreading wave during a specific ictal event. We selected a set of points $i = 1,\ldots, n$ in the structure involved (cortex or thalamus) and plotted the cumulative distances x_i versus the delays t_i (**Supplementary Fig. 3c**). The velocity was given by the slope of this curve calculated using a linear regression. The error on the slope was given by the s.d. of the slope coefficient

$$\delta a = \sqrt{\frac{1}{n-1}\frac{\sum_{i=1}^{n}(x_i - \tilde{x}_i)^2}{\sum_{i=1}^{n}(t_i - \hat{t})^2}}, \qquad \tilde{x}_i = at_i + b$$

where a and b are the coefficients of the linear regression and ^ designates the mean value.

Animal handling and surgery. All animals received humane care in compliance with the European Communities Council Directive of 24 November 1986 (86/609/EEC), and the study was approved by the institutional and regional committees for animal care. We anesthesized adult (>3-week-old) Sprague-Dawley rats with

isoflurane (3% for initiation, 0.5% for maintenance) in 100% O_2. An equal number of male and female rats were used in each experiment. We placed the head in a stereotaxic apparatus, incised the skin and drilled a large cranial window[18]. The window ranged from bregma to lambda and was 12 mm wide laterally (coordinates from β +6 mm to β −6 mm)[17]. It was necessary to remove the bone to allow undistorted propagation of ultrasound waves between probe and tissue. We chose to open a large window in order to observe the whole brain. However, it would be possible to image a smaller portion of the brain through a smaller craniotomy, with the only limitation being that the window must be wider than the width of the ultrasonic beam in the direction perpendicular to the imaging plane (which depends on the probe's characteristics). We took care not to damage the dura to prevent inflammatory processes in the brain. We formed a ridge around the window with dental cement to allow us to cover the brain with a viscous isotonic solution (0.4% xanthan gum) that ensured acoustic transmission. We aligned the ultrasonic probe in the coronal plane 2 mm above the brain. A motorized arm moved it along the anteroposterior axis. We kept the temperature of the rat at 37 °C with a heating blanket controlled by rectal probe feedback and monitored the rats by electrocardiogram.

Whisker stimulation. To excite the facial whiskers, we used a small comb controlled by an electromagnetic actuator (linear solenoid, Saia-Burgess). We placed it 1 cm away from the rat muzzle and deflected the whiskers (5-mm amplitude) in the caudal direction at a frequency of 12 Hz. The stimulation pattern consisted of ten cycles (32 s on/64 s off). For experiments involving single whisker stimulation, we cut all the whiskers except for one, chosen in row C or D.

Induction of seizures. We induced epileptiform activities by a focal injection of 1 µl 4-aminopyridine (4-AP; Sigma-Aldrich) solution at a concentration of 15 mmol l^{-1}, through a 150-µm-diameter cannula that we inserted 1 mm deep into the cortex under ultrasonic guidance. We monitored neuronal activity with eight electrodes made of polyimide-insulated 100-µm-diameter nickel-chrome wire (California Fine Wire) implanted in the cortex at different locations in the imaging plane. We recorded the signals with a Digital Lynx EEG amplifier and acquisition system (Neuralynx). For the comparison between power Doppler and electric signals, the row of eight electrodes was placed under ultrasonic guidance in the coronal plane imaged by the ultrasonic probe. We matched the position of the tip of the electrode with the corresponding imaging pixel, and the power Doppler signal was averaged on a 3 × 3–pixel area around this pixel. Electrodes were positioned 1 mm below the surface of the cortex, regularly spaced by about 1.5–2.0 mm along the *x* axis.

16. Angelsen, B.A.J. in *Ultrasound Imaging* Vol. 2, 10.3–10.46 (Emantec, 2000).
17. Paxinos, G. & Watson, C. *The Rat Brain in Stereotaxic Coordinates* 4th edn. (Academic Press, New York, 1998).
18. Mostany, R. & Portera-Cailliau, C. *J. Vis. Exp.* **12**, 680–681 (2008).

doi:10.1038/nmeth.1641